21-cm cosmology in the 21st Century

Pritchard & Loeb , arXiv:1109.6012

Journal Club Cosmologie
SAP/SPP/IPHT
28 Octobre 2014

R. Ansari - Univ. paris-Sud, LAL - CNRS/IN2P3

21-cm cosmology in the 21st Century

Jonathan R. Pritchard and Abraham Loeb

Institute for Theory & Computation, Harvard University, 60 Garden St., Cambridge, MA 02138, USA

E-mail: `jpritchard@cfa.harvard.edu; aloeb@cfa.harvard.edu`

Abstract.

Imaging the Universe during the first hundreds of millions of years remains one of the exciting challenges facing modern cosmology. Observations of the redshifted 21 cm line of atomic hydrogen offer the potential of opening a new window into this epoch. This will transform our understanding of the formation of the first stars and galaxies and of the thermal history of the Universe. A new generation of radio telescopes is being constructed for this purpose with the first results starting to trickle in. In this review, we detail the physics that governs the 21 cm signal and describe what might be learnt from upcoming observations. We also generalize our discussion to intensity mapping of other atomic and molecular lines.

Jonathan R. Pritchard & Abraham Loeb , Rep. Prog. Phys. 75 , 086901 (2012)
arXiv:1109.6012

1. L'émission à 21 cm
2. L'évolution cosmique de l'hydrogène
3. Intensity mapping

Contents

Jonathan R. Pritchard & Abraham Loeb , Rep. Prog. Phys. 75 , 086901 (2012)
arXiv:1109.6012

Rayonnement à 21 cm

- Niveaux atomiques: >100 THz (visible, UV), vibrations moléculaires (0.1…100 THz), rotation moléculaires (10…1000 GHz)
- Effets électroniques collectifs : kHz … 10 GHz
- Niveau hyperfine de l'hydrogène atomique : transition de spin (spin-flip) de l'électron dans le champ magnétique du moment dipolaire du noyau

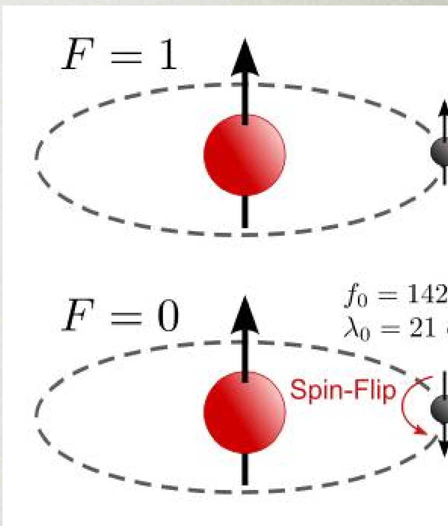

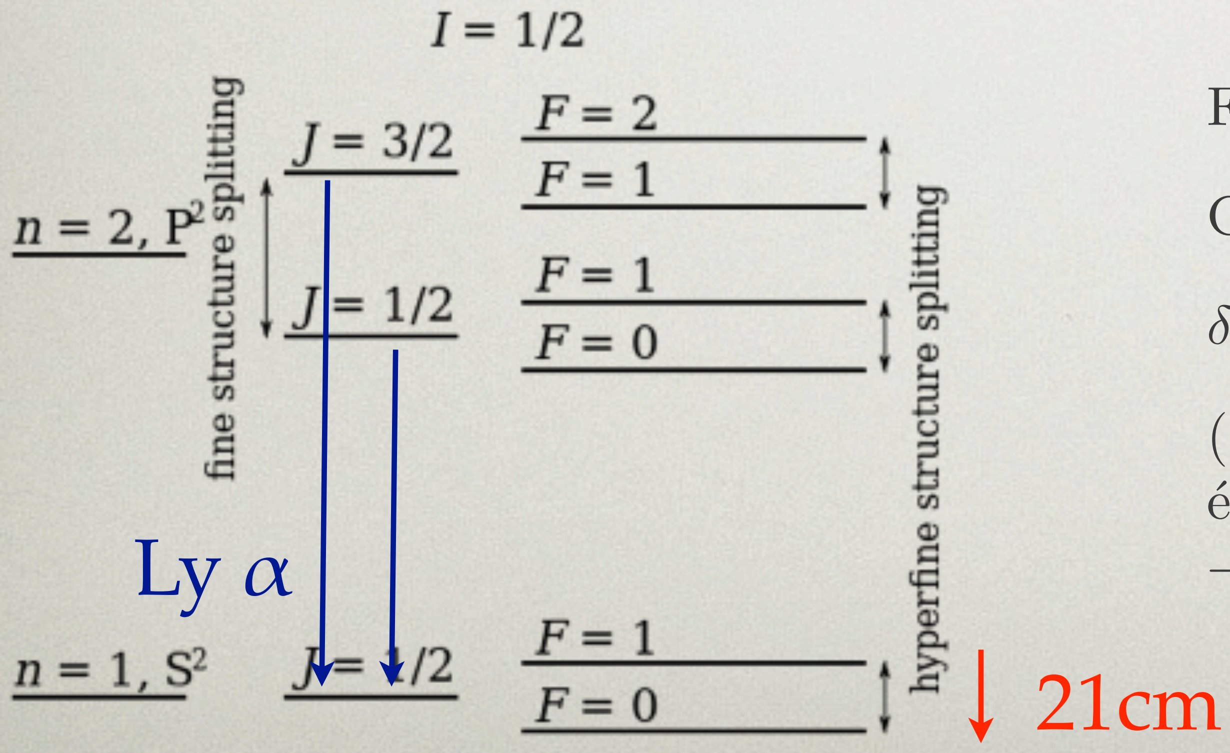

Fréquence d'émission : $\nu_{21} = 1.4204\ 10^9$ Hz

Coefficient émission spontanée : $A_{21} = 2.87\ 10^{-15}\ s^{-1}$

$\delta T_{21} = h\nu_{21}/k \simeq 0.0682\mathrm{K} \ll T_{CMB} = 2.725\,\mathrm{K}$

(+) triplet, (-) singulier et le niveau inférieur un singulet. équirépartition des atomes sur (+)/(-) si $T_s \gg \delta T_{21}$
$\rightarrow N^+ = 3/4\ N_{H_I}$.

HI à travers l'histoire cosmique

NOTES

ON THE DENSITY OF NEUTRAL HYDROGEN IN INTERGALACTIC SPACE

Recent spectroscopic observations by Schmidt (1965) of the quasi-stellar source 3C 9, which is reported by him to have a redshift of 2.01, and for which Lyman-α is in the visible spectrum, make possible the determination of a new very low value for the density of neutral hydrogen in intergalactic space. It is observed that the continuum of the source continues (though perhaps somewhat weakened) to the blue of Ly-α; the line as seen on the plates has some structure but no obvious asymmetry. Consider, however, the fate of photons emitted to the blue of Ly-α. As we move away from the source along the line of sight, the source becomes redshifted to observers locally at rest in the expansion, and for one such observer, the frequency of any such photon coincides with the rest frequency of Ly-α in his frame and can be scattered by neutral hydrogen in his vicinity.

• • •

The flux can come from three sources; normal galaxies, radiogalaxies, and QSS's, and the intergalactic medium itself. The contribution from the first two sources can be estimated roughly, and almost certainly does not exceed 3×10^{-24} units at $z = 2$, of which about 10 per cent is from quasi-stellar sources (assuming that one can extrapolate the visual radiation into the *UV* with a spectral index of -0.7, and assuming a present space density of $[600 \text{ Mpc}]^{-3}$).

• • •

We would like to express our sincere thanks to Dr. Maarten Schmidt, who kindly put the 3C 9 plates at our disposal for measurement. The qualitative conclusions in the present version of this paper are in agreement with the analysis of Dr. J. Bahcall and Dr. E. Salpeter (to be published). We are indebted to Dr. J. Bahcall and Dr. E. Salpeter and also Dr. D. Sciama for pointing out numerical errors in the circulated preprint. This work was supported by the National Science Foundation and the National Aeronautics and Space Administration.

James E. Gunn
Bruce A. Peterson

May 26, 1965; revised July 26 and in proof on October 8, 1965

Mount Wilson and Palomar Observatories
Carnegie Institution of Washington
California Institute of Technology

REFERENCES

Allen, C. W. 1963, *Astrophysical Quantities* (London: Athlone Press).
Field, G. 1962, *Ap. J.*, **135**, 684.
Field, G., and Henry, R. 1964, *Ap. J.*, **140**, 1002.
Karzas, W., and Latter, R. 1961, *Ap. J. Suppl.*, **6**, 167.
Sandage, A. 1961*a*, *Ap. J.*, **133**, 355.
———. 1961*b*, *ibid.*, **134**, 916.
Schmidt, M. 1965, *Ap. J.*, **141**, 1295.

James E. Gunn & Bruce A. Peterson
ApJ. vol 142 , p. 1633-1641 (11/1965)

Illustration : Scientific American, April 2014

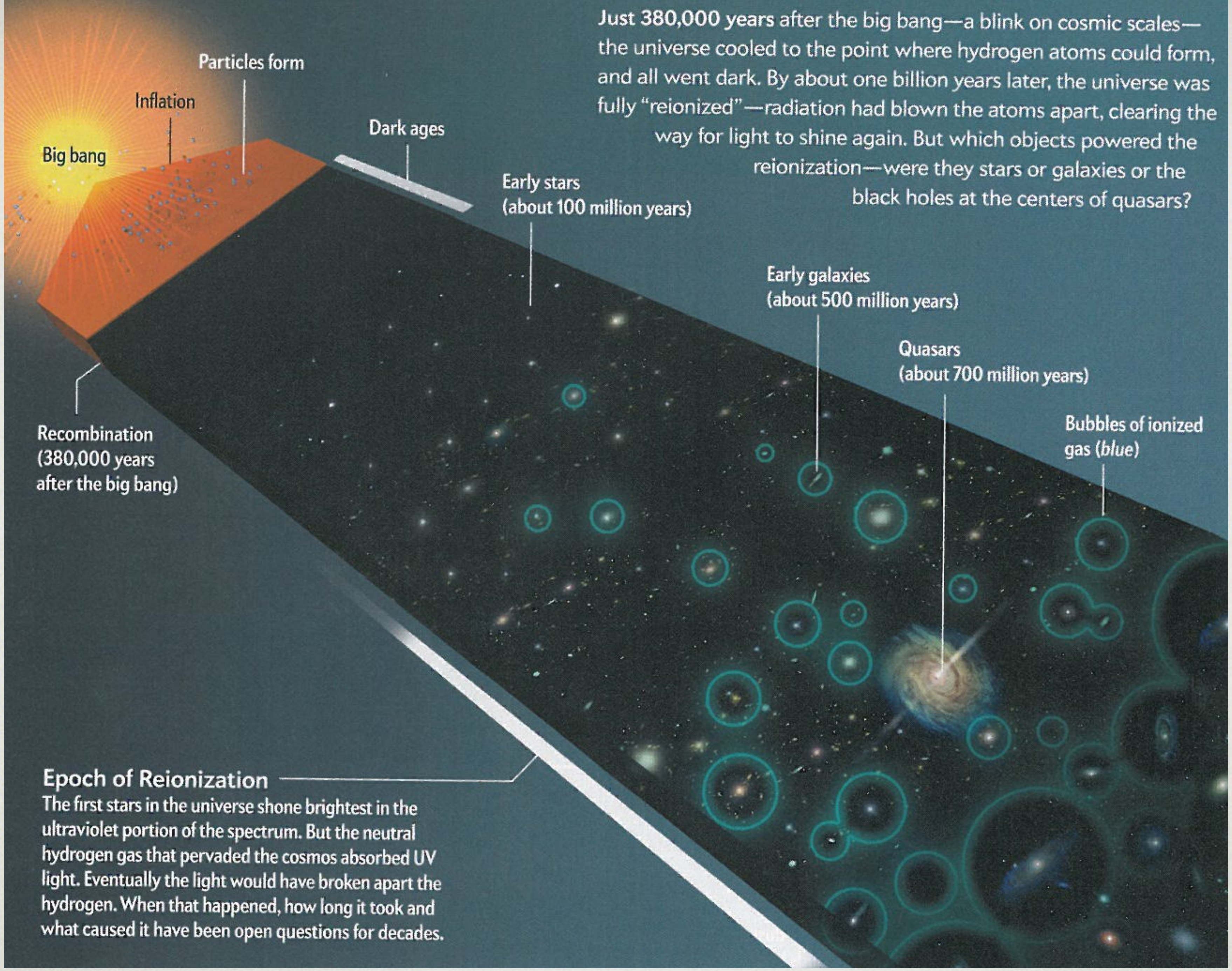

Reionisation

	Dark ages		**First stars / Galaxies ...**		**Quasars ...**	**Today**
$n_b\ (cm^{-3})$	330	0.25	0.03	$3.\,10^{-4}$	$5.\,10^{-5}$	$2.5\,10^{-7}$
Age (MY)	0.38	15	50	500	1200	13800
T (K)	3000	300	150	30	15	2.725
z	1100	100	50	10	5	0

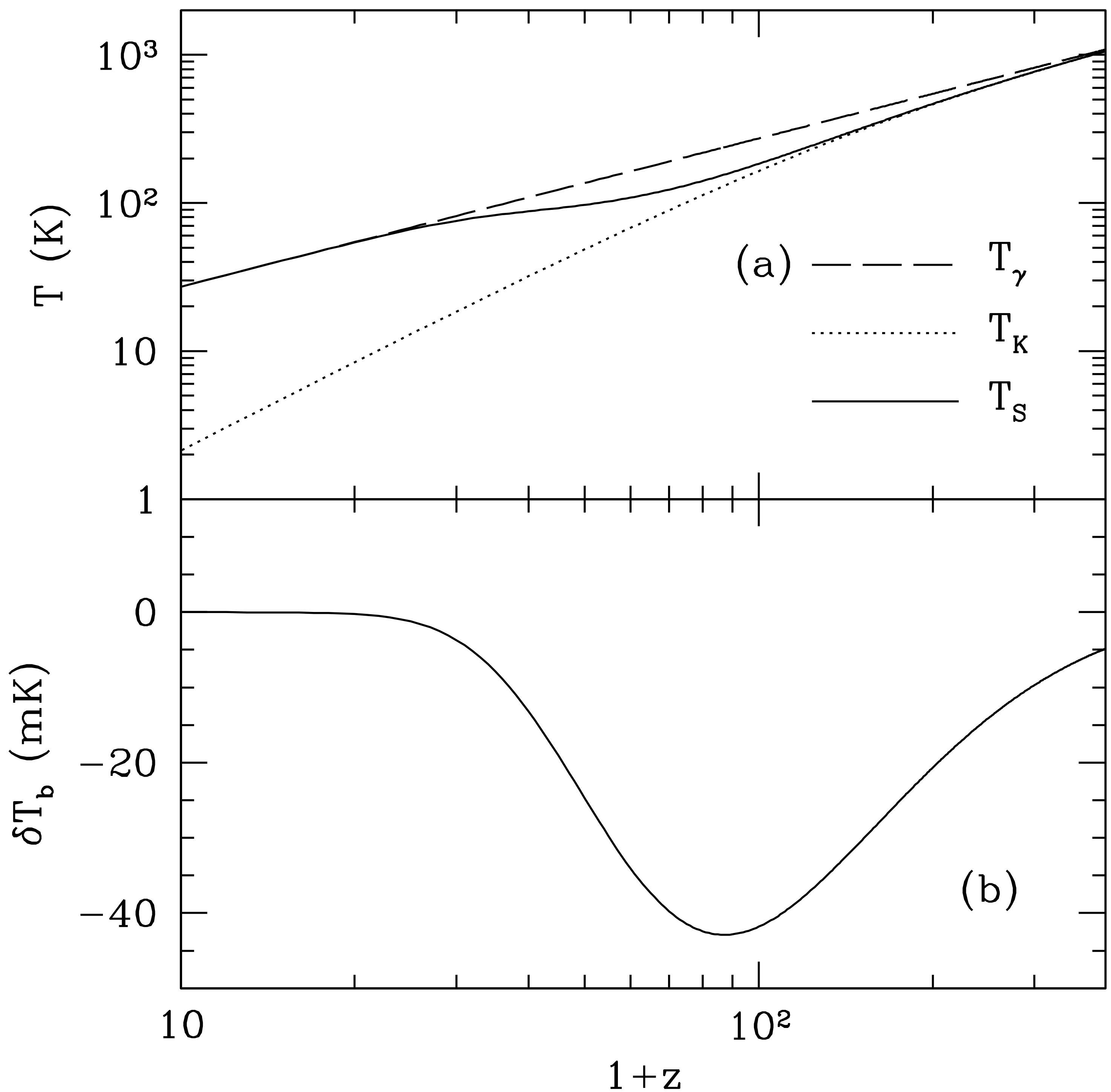

S. Furlanetto, S. Peng Ho, F. Briggs, Phys.Rept. 433 (2006) , arXiv:0608032

température du rayonnement (CMB) $T\gamma$

$$T_\gamma \propto (1+z)$$

Température cinétique du gaz (Hydrogène neutre) TK

$$T_K \propto (1+z)^2$$

Température de spin TS

$$\begin{aligned} \frac{n_+}{n_-} &= \frac{g_+}{g_-} \exp\left(-\frac{E_{21}}{kT_S}\right) \\ &= 3 \exp\left(-\frac{T_*}{T_S}\right) \\ T_* &\simeq 0.068K \end{aligned}$$

Pas de signal à 21 cm si TS = $T\gamma$

si observé sur le fond diffus (CMB)

Mécanisme de couplage T_K T_S

(température cinétique, température de spin)

- diffusion compton des photons (CMB) sur les électrons résiduels (z>~200)
- Collisions entre atomes d'hydrogène - diminue lorsque la densité baisse
- Effet Wouthuysen-Field : population deux deux états de spin à travers des transitions Lyman, dans un bain de photons UV
- Le gaz (hydrogène atomique) est plus froid que le gaz de photons (CMB), sauf lorsqu'il est réchauffé par le rayonnement X émis des étoiles très massives/quasars …

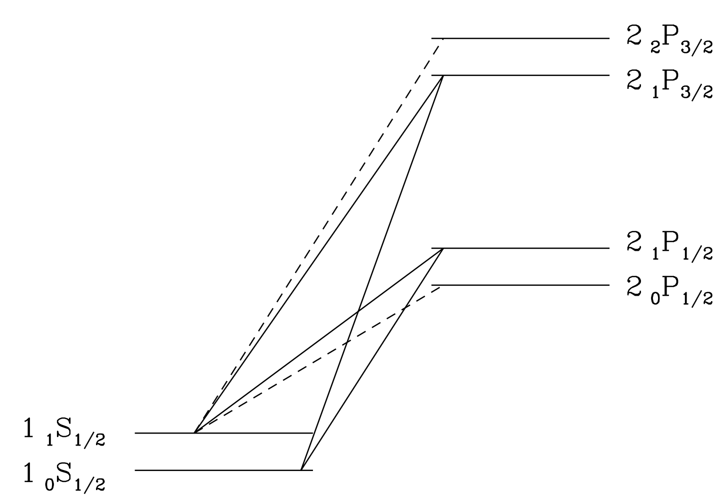

S. Furlanetto, S. Peng Ho, F. Briggs, Phys.Rept. 433 (2006)

J. Pritchard, S. Furlanetto, MNRAS (2006)

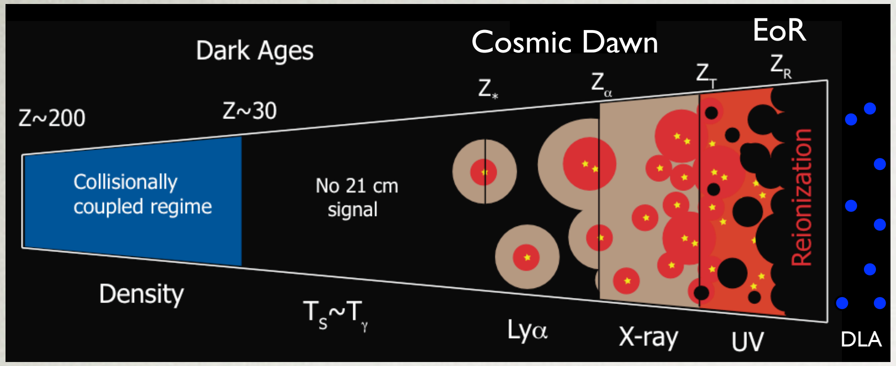

Figure 3. Cartoon of the different phases of the 21 cm signal. The signal transitions from an early phase of collisional coupling to a later phase of Lyα coupling through a short period where there is little signal. Fluctuations after this phase are dominated successively by spatial variation in the Lyα , X-ray, and ionizing UV radiation backgrounds. After reionization is complete there is a residual signal from neutral hydrogen in galaxies.

- $\mathbf{200 \lesssim z \lesssim 1100}$: The residual free electron fraction left after recombination allows Compton scattering to maintain thermal coupling of the gas to the CMB, setting $T_K = T_\gamma$. The high gas density leads to effective collisional coupling so that $T_S = T_\gamma$ and we expect $\bar{T}_b = 0$ and no detectable 21 cm signal.
- $\mathbf{40 \lesssim z \lesssim 200}$: In this regime, the gas cools adiabatically so that $T_K \propto (1+z)^2$ leading to $T_K < T_\gamma$ and collisional coupling sets $T_S < T_\gamma$, leading to $\bar{T}_b < 0$ and an early absorption signal. At this time, T_b fluctuations are sourced by density fluctuations, potentially allowing the initial conditions to be probed [32, 22].
- $\mathbf{z_\star \lesssim z \lesssim 40}$: As the expansion continues, decreasing the gas density, collisional coupling becomes ineffective and radiative coupling to the CMB sets $T_S = T_\gamma$, and there is no detectable 21 cm signal.
- $\mathbf{z_\alpha \lesssim z \lesssim z_\star}$: Once the first sources switch on at $z_\star$, they emit both Lyα photons and X-rays. In general, the emissivity required for Lyα coupling is significantly less than that for heating T_K above T_γ. We therefore expect a regime where the spin temperature is coupled to cold gas so that $T_S \sim T_K < T_\gamma$ and there is an absorption signal. Fluctuations are dominated by density fluctuations and variation in the Lyα flux [33, 24, 34]. As further star formation occurs the Lyα coupling will eventually saturate ($x_\alpha \gg 1$), so that by a redshift z_α the gas will everywhere be strongly coupled.
- $\mathbf{z_h \lesssim z \lesssim z_\alpha}$: After Ly$\alpha$ coupling saturates, fluctuations in the Lyα flux no longer affect the 21 cm signal. By this point, heating becomes significant and gas temperature fluctuations source T_b fluctuations. While T_K remains below T_γ we see a 21 cm signal in absorption, but as T_K approaches T_γ hotter regions may begin to be seen in emission. Eventually by a redshift z_h the gas will be heated everywhere so that $\bar{T}_K = T_\gamma$.
- $\mathbf{z_T \lesssim z \lesssim z_h}$: After the heating transition, $T_K > T_\gamma$ and we expect to see a 21 cm signal in emission. The 21 cm brightness temperature is not yet saturated, which occurs at z_T, when $T_S \sim T_K \gg T_\gamma$. By this time, the ionization fraction has likely risen above the percent level. Brightness temperature fluctuations are sourced by a mixture of fluctuations in ionization, density and gas temperature.
- $\mathbf{z_r \lesssim z \lesssim z_T}$: Continued heating drives $T_K \gg T_\gamma$ at z_T and temperature fluctuations become unimportant. $T_S \sim T_K \gg T_\gamma$ and the dependence on T_S may be neglected in equation (7), which greatly simplifies analysis of the 21 cm power spectrum [35]. By this point, the filling fraction of HII regions probably becomes significant and ionization fluctuations begin to dominate the 21 cm signal [36].
- $\mathbf{z \lesssim z_r}$: After reionization, any remaining 21 cm signal originates primarily from collapsed islands of neutral hydrogen (damped Lyα systems).

Baisse de densité: T_S s'équilibre avec T_γ

Chauffage du gaz (photons X) - augmentation de T_K donc de T_S

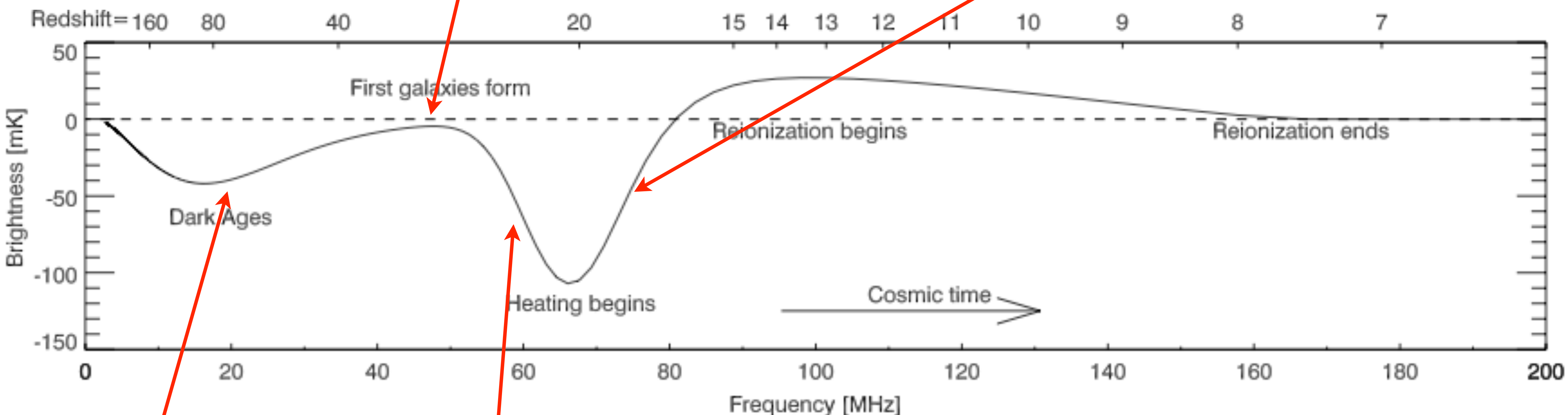

A. Liu, J.R. Pritchard, M. tegmark, A. Loeb. (2012) , arXiv:1211.3743

Couplage $T_S \leftrightarrow T_K$ à travers les collisions

Couplage $T_S \leftrightarrow T_K$ à travers l'effet Wouthuysen-Field, dans le bain des photons UV des premières étoiles

J.R. Pritchard, A. Loeb. (2010) , arXiv:1005.4057

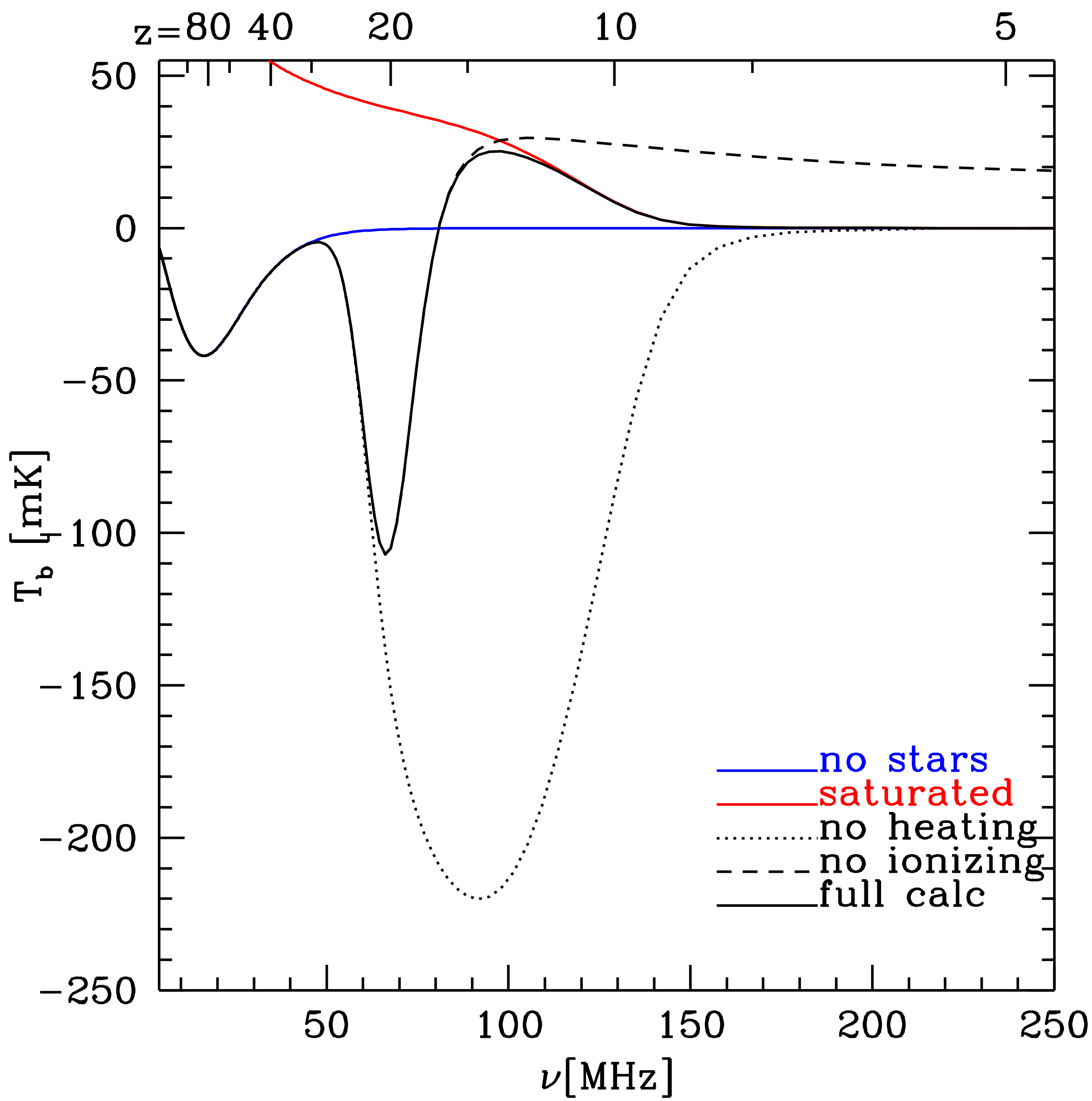

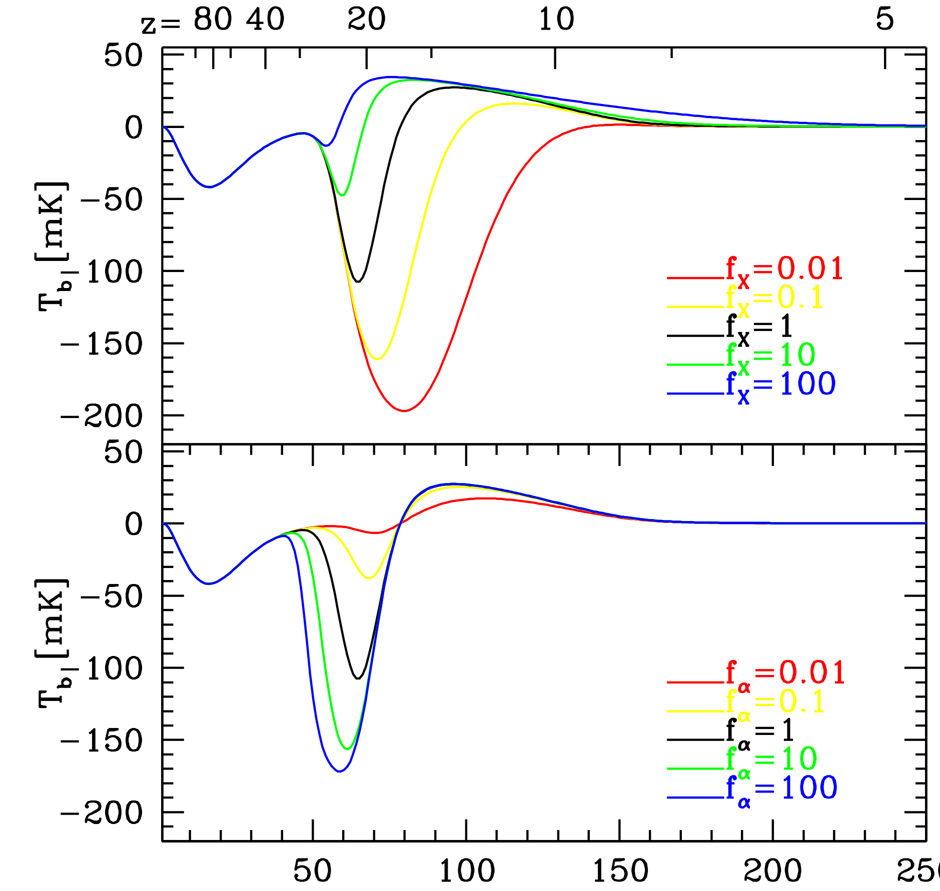

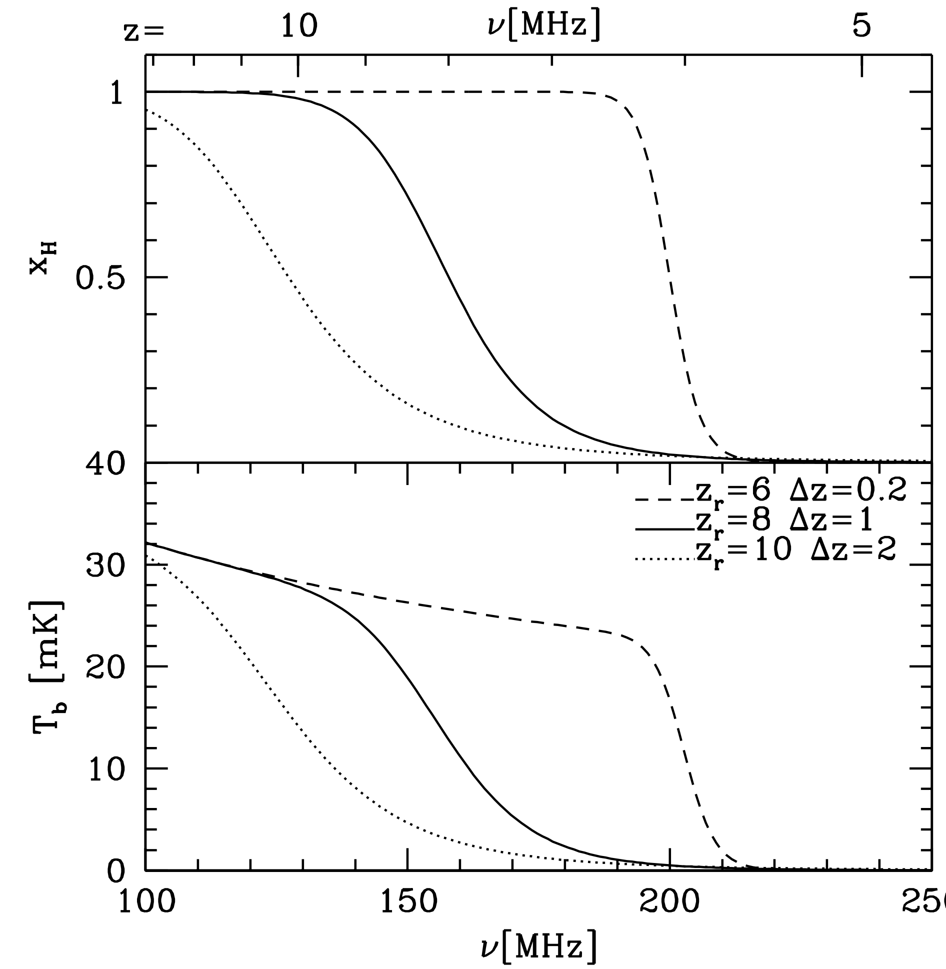

Évolution de la température de brillance du gaz HI avec le redshift

FIG. 6: Evolution of the neutral fraction x_H and brightne
temperature T_b for a *tanh* model of reionization (see Eq.8)

Planck 2013 results. XVI. Cosmological parameters

Planck Collaboration: Cosmological parameters

	Planck		*Planck*+lensing		*Planck*+WP	
Parameter	Best fit	68% limits	Best fit	68% limits	Best fit	68% limits
$\Omega_b h^2$	0.022068	0.02207 ± 0.00033	0.022242	0.02217 ± 0.00033	0.022032	0.02205 ± 0.00028
$\Omega_c h^2$	0.12029	0.1196 ± 0.0031	0.11805	0.1186 ± 0.0031	0.12038	0.1199 ± 0.0027
$100\theta_{MC}$	1.04122	1.04132 ± 0.00068	1.04150	1.04141 ± 0.00067	1.04119	1.04131 ± 0.00063
τ	0.0925	0.097 ± 0.038	0.0949	0.089 ± 0.032	0.0925	$0.089^{+0.012}_{-0.014}$
n_s	0.9624	0.9616 ± 0.0094	0.9675	0.9635 ± 0.0094	0.9619	0.9603 ± 0.0073
$\ln(10^{10} A_s)$	3.098	3.103 ± 0.072	3.098	3.085 ± 0.057	3.0980	$3.089^{+0.024}_{-0.027}$

Optical depth obtained from CMB : integral measurement of the ionization fraction

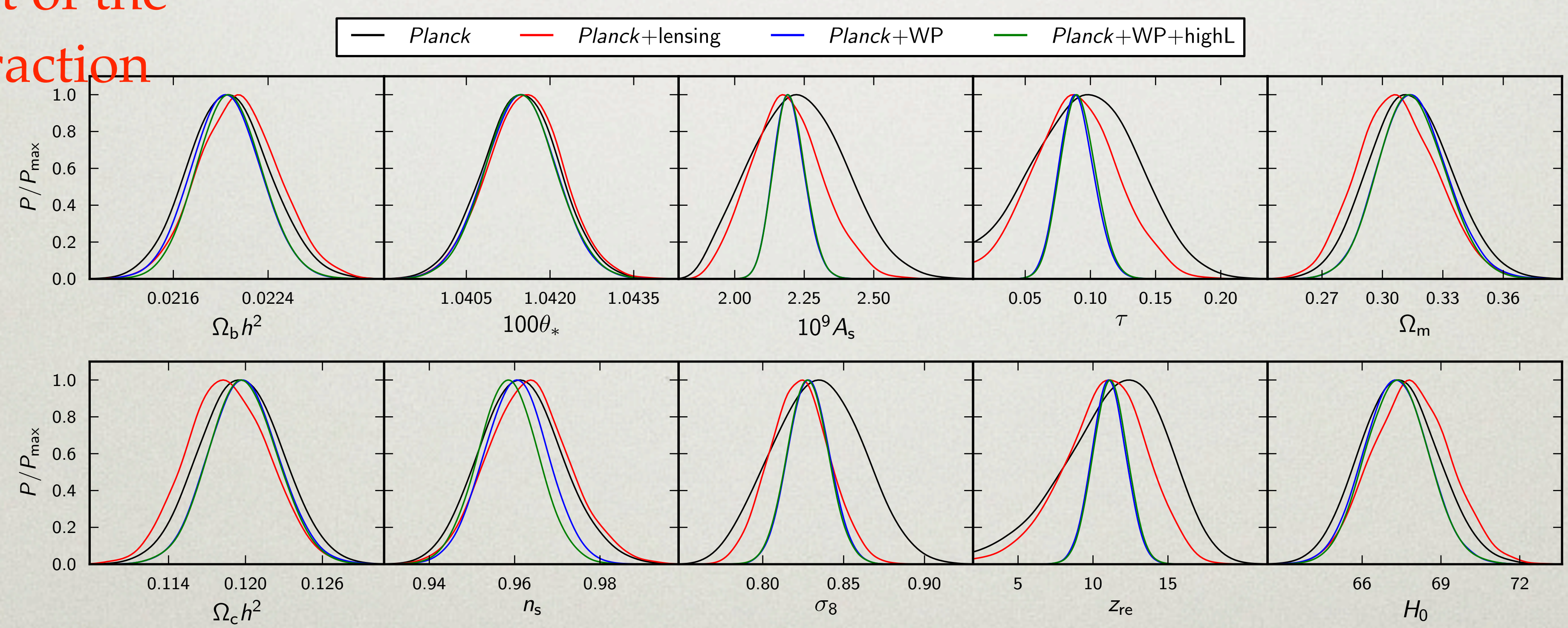

Fig. 4. Marginalized constraints on parameters of the base ΛCDM model for various data combinations.

21 cm tomography

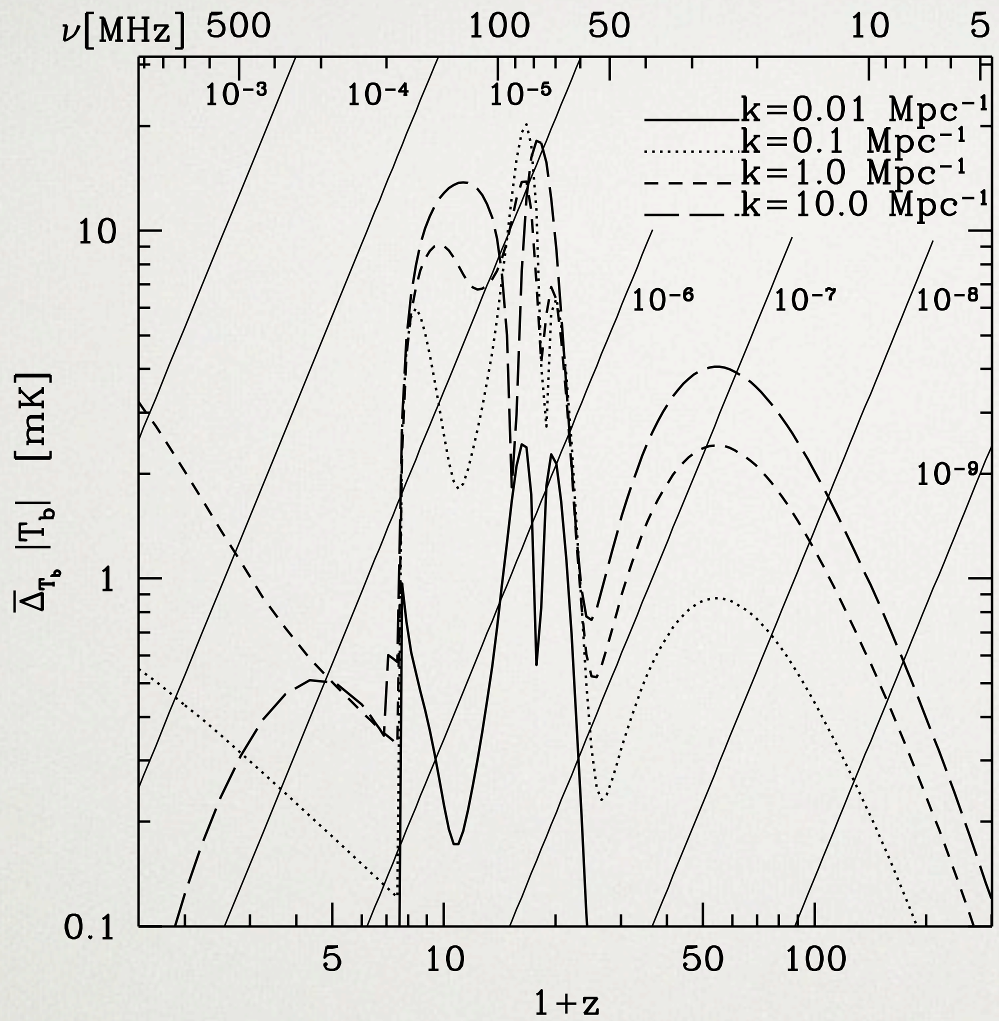

Figure 8. Evolution of power spectrum fluctuations. The different curves show $P(k, z)$ as a function of z at fixed k for $k = 0.01,\ 0.1,\ 1,\ 10\ \mathrm{Mpc}^{-1}$. Diagonal lines show $\epsilon T_{\mathrm{fg}}(\nu)$, the foreground temperature reduced by a factor ϵ ranging from $10^{-3} - 10^{-9}$ to indicate the level of foreground removal required to detect the signal [78].

21cm signal power spectrum as a function of redshift : LOFAR, MWA, SKA …

The LOFAR observatory

- **LBA** (10) 30 - 90 MHz — **HBA** 115 - 240 MHz
- isolated dipoles — tiles (4x4 dipoles)

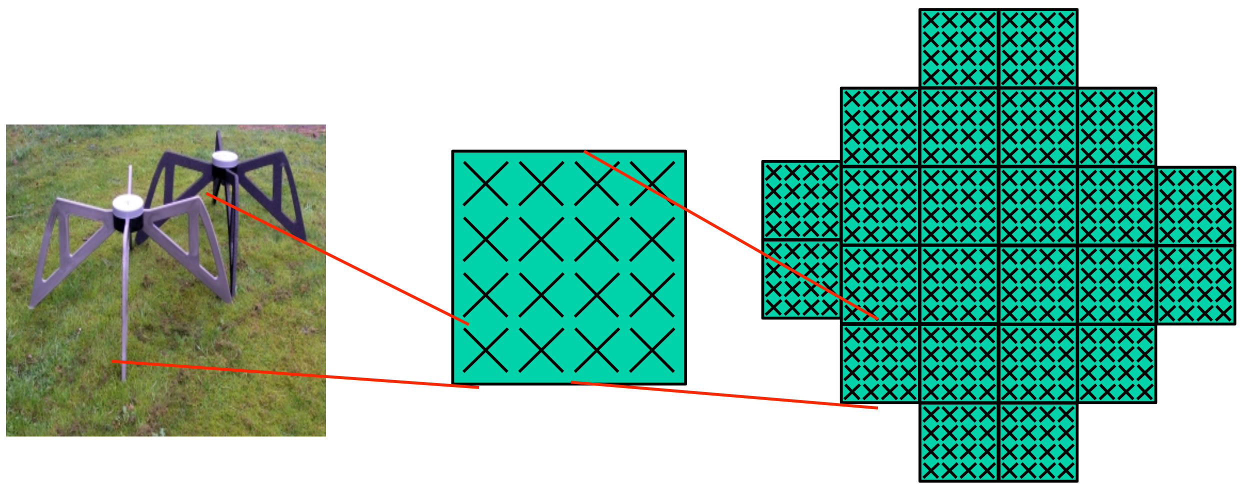

Core	2 km	23+ stations
NL	80 km	18+ stations
Europe	>1000 km	8+ stations

Total # of HBA dipoles: ~ 50000.

Timeline:
1. Official opening: June 2010
2. Data for our project starts: Dec. 2012
3. First results (hopefully) 2014

Slide borrowed from S. Zaroubi

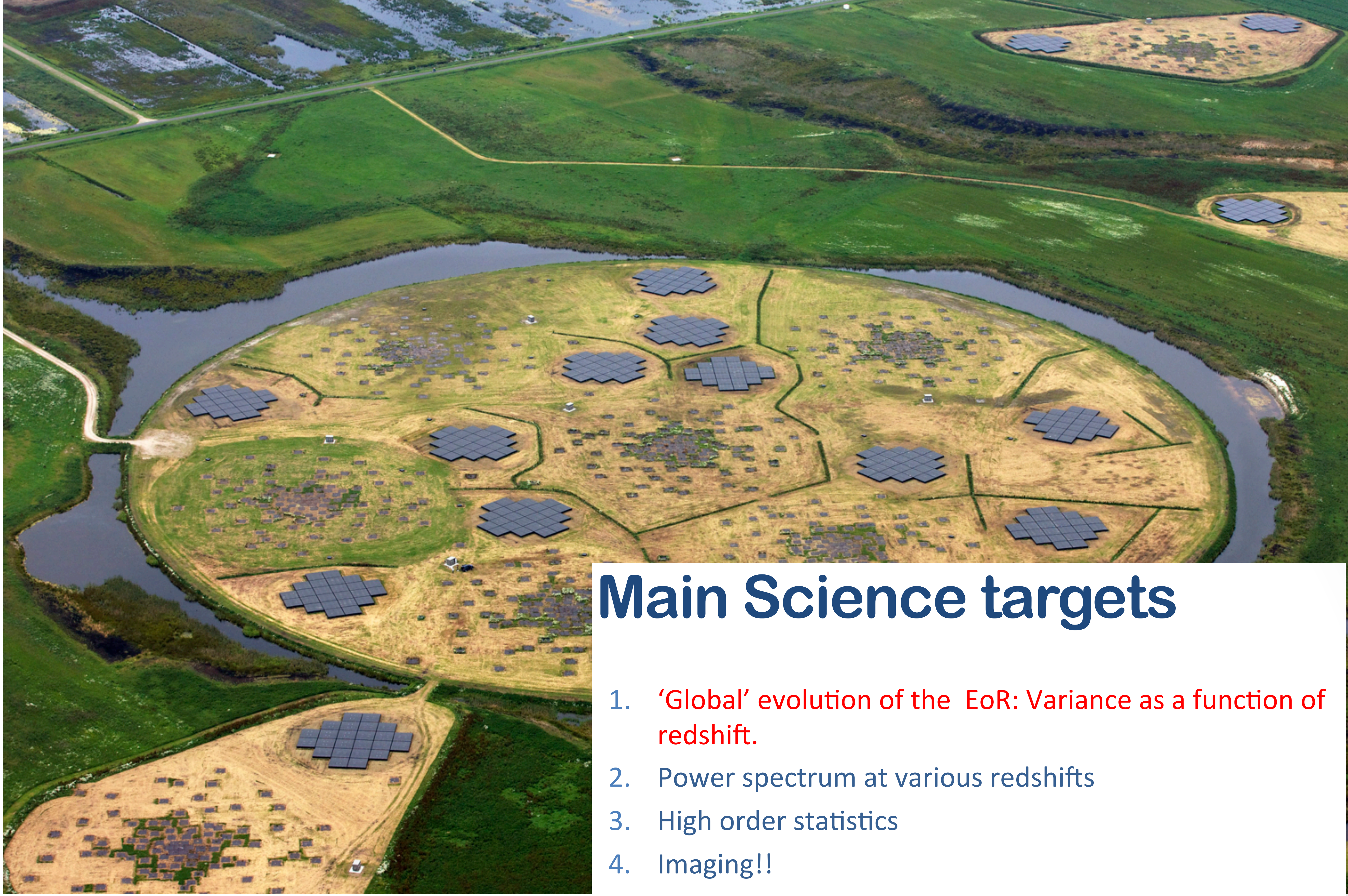

Main Science targets

1. 'Global' evolution of the EoR: Variance as a function of redshift.
2. Power spectrum at various redshifts
3. High order statistics
4. Imaging!!

LOFAR

5. Cross-correlation with other probes
6. The 21 cm forest

Intensity mapping

Intensity mapping T21(α,δ,z)

- 3D mapping of neutral hydrogen distribution through total 21 cm radio emission (no source detection)
- Needs only a modest angular resolution 10-15 arcmin
- Needs a large instantaneous field of view (FOV) and bandwidth (BW)

≡ Instrument noise (Tsys)

≡ Foregrounds / radio sources and component separation

- Peterson, Bandura & Pen (2006)
- Chang et al. (2008) arXiv:0709.3672
- Ansari et al (2008) arXiv:0807.3614
- Wyithe, Loeb & Geil (2008) arXiv:0709.2955
- Peterson et al (2009) arXiv:0902.3091
- Ansari et al (2012) arXiv:1108.1474

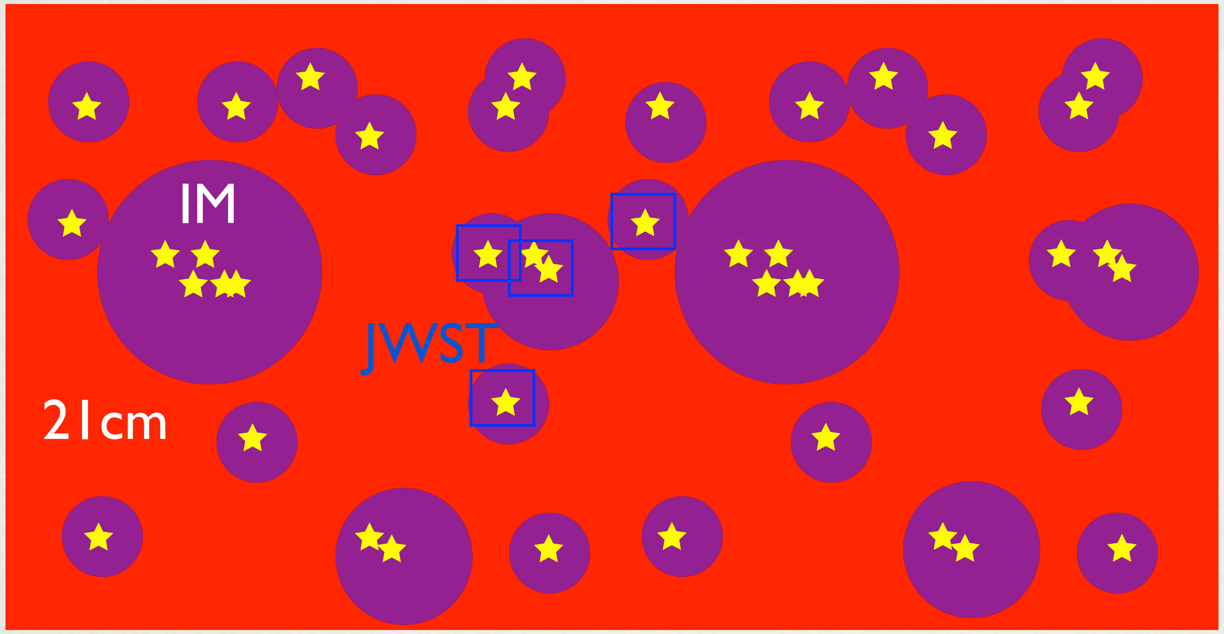

Figure 12. Cartoon of the role intensity mapping would play in understanding galaxy formation. Deep galaxy surveys with HST and JWST image the properties of individual galaxies in small fields (blue boxes). 21 cm tomography (red filled region) provides a "negative space" view of the Universe by determining the properties of the neutral gas surrounding groups of galaxies. Intensity mapping (purple filled regions) fills in the gaps providing information about the collective properties of groups of galaxies. Together the three would give a complete view of the early generation of galaxies in the infant universe.

Cross-correlating information from intensity mapping surveys and deep galaxy surveys with HST and JWST

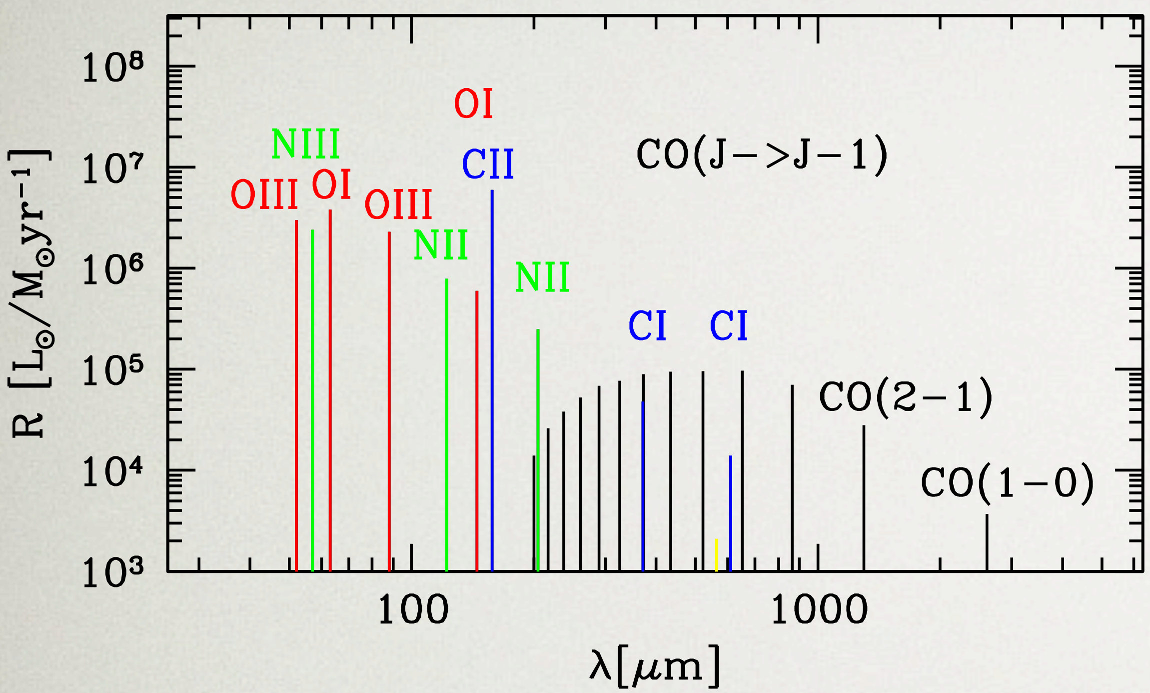

Figure 13. Ratio between line luminosity, L, and star formation rate, $\dot{M}_*$, for various lines observed in galaxies and taken from Table 1 of Ref. [170]. For the first 7 lines this ratio is measured from a sample of low redshift galaxies. The other lines have been calibrated based on the galaxy M82. Some weaker lines, for example for HCN, have been omitted for clarity.

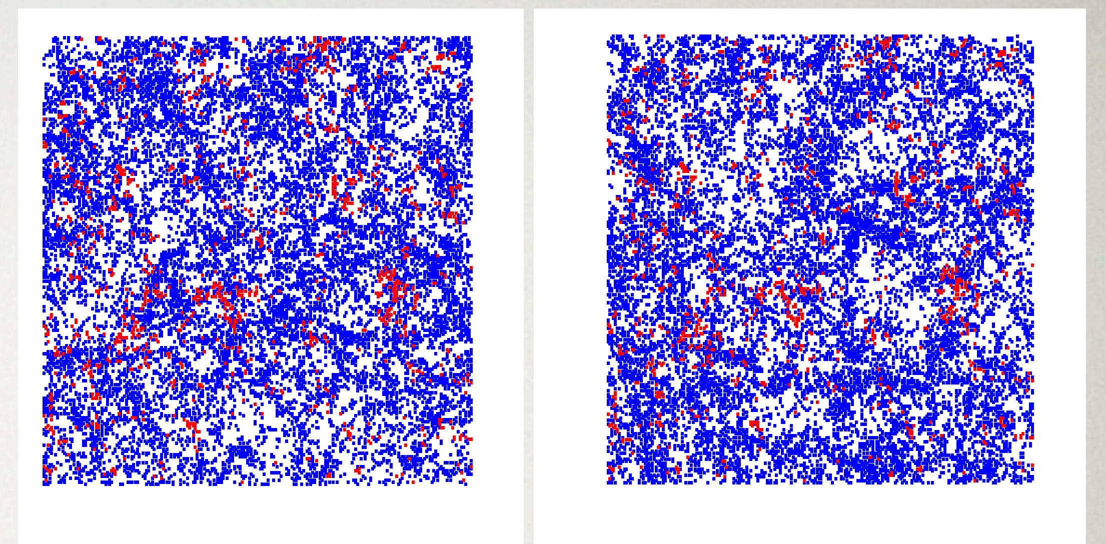

Figure 14. A slice from a simulated realization of line emission from galaxies at an observed wavelength of 441μm (left) and 364μm (right) [170]. The slice is in the plane of the sky and spans 250×250 comoving Mpc^2 with a depth of $\Delta\nu/\nu = 0.001$. The colored squares indicate pixels which have line emission greater than 200Jy/Sr for the left panel and 250Jy/Sr for the right panel. The emission from OI(63μm) and OIII(52μm) is shown in red on the left and right panels, respectively, originating from the same galaxies at $z = 6$. All of the lines illustrated in Figure 13 are included and plotted in blue. Cross correlating data at these two observed wavelengths would reveal the emission in OI and OIII from $z = 6$ with the other emission lines being essentially uncorrelated.

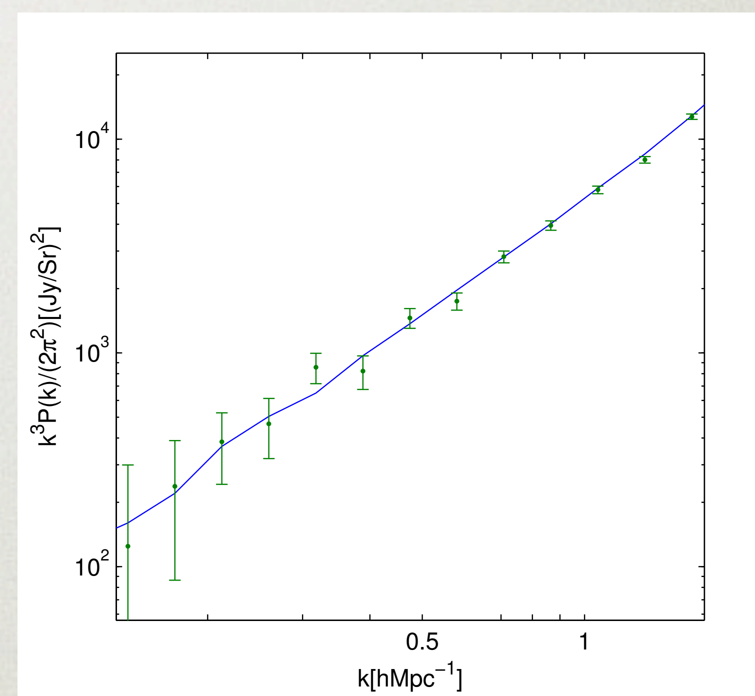

Figure 15. The cross power spectrum of OI(63 μm) and OIII(52 μm) at $z = 6$ measured from mock simulation data for a hypothetical infrared space telescope similar to SPICA [170]. The solid line is the cross power spectrum measured when only line emission from galaxies in the target lines is included. The points are the recovered power spectrum when detector noise, contaminating line emission, galaxy continuum emission, and dust in our galaxy and the CMB are included. The error bars follow Eq. (62) with $P_{1\mathrm{total}}$ and $P_{2\mathrm{total}}$ calculated from the simulated data, including detector noise, contaminating line emission and sample variance.

Intensity mapping with molecular (CO, …) lines … using cross correlations between different frequencies

21cm forest

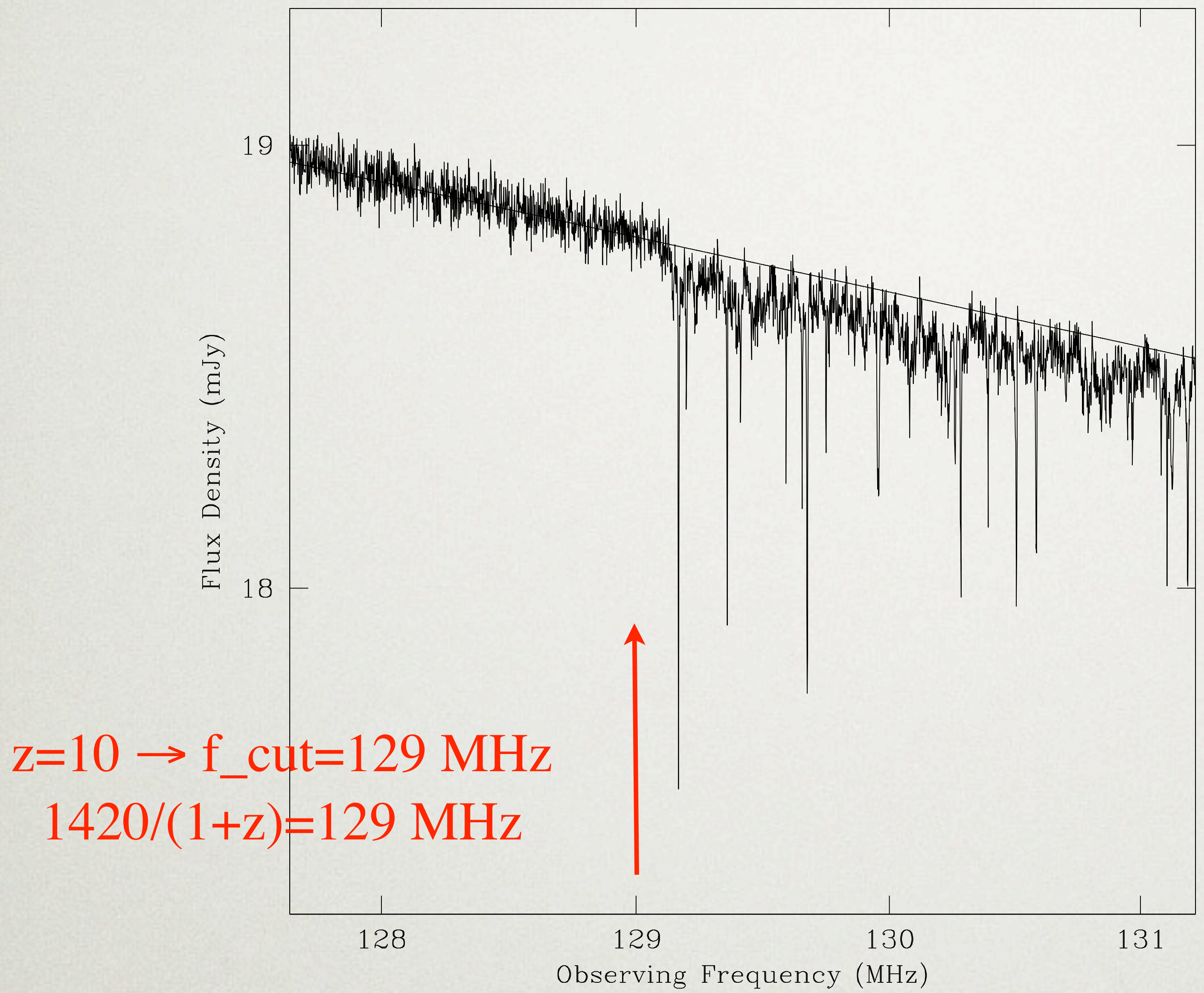

Probing Hydrogen gas (in absorption) using quasar line of sight

Figure 19. Simulated spectrum from 128 to 131 MHz of a source with brightness $S(120\,\mathrm{MHz}) = 20\,\mathrm{mJy}$ at $z = 10$ using a model spectrum based on that of Cygnus A and assuming HI 21 cm absorption by the IGM. Thermal noise has been added using the specifications of the square kilometer array (SKA) and assuming 10 days integration with 1 kHz wide spectral channels. The solid line is the model spectrum without noise or absorption [181].

Prospects

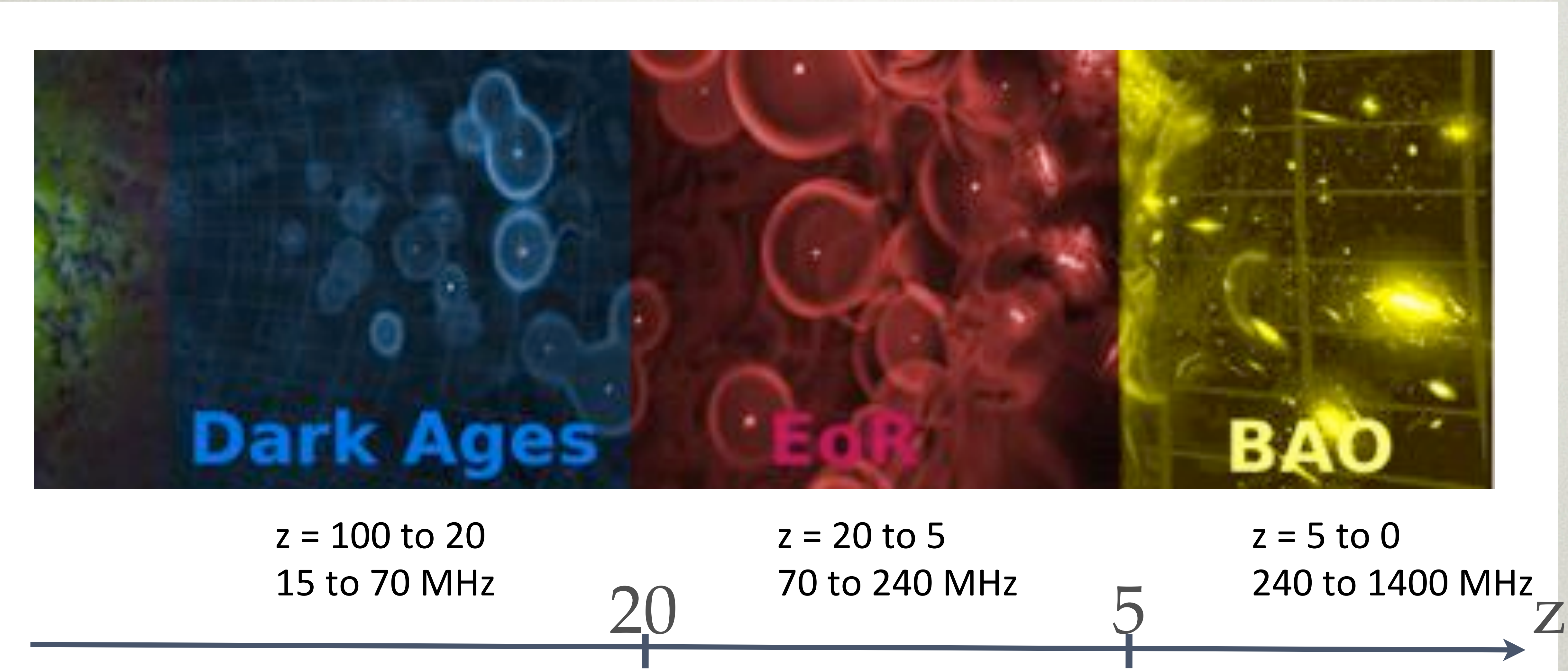

- LOFAR
- GMRT
- MWA

- SKA-LOW
- HERA

- **CHIME**
- **Tianlai**
- GBT
- BAOBab
- BINGO

+ global 21cm signal experiments : EDGES, CoRE

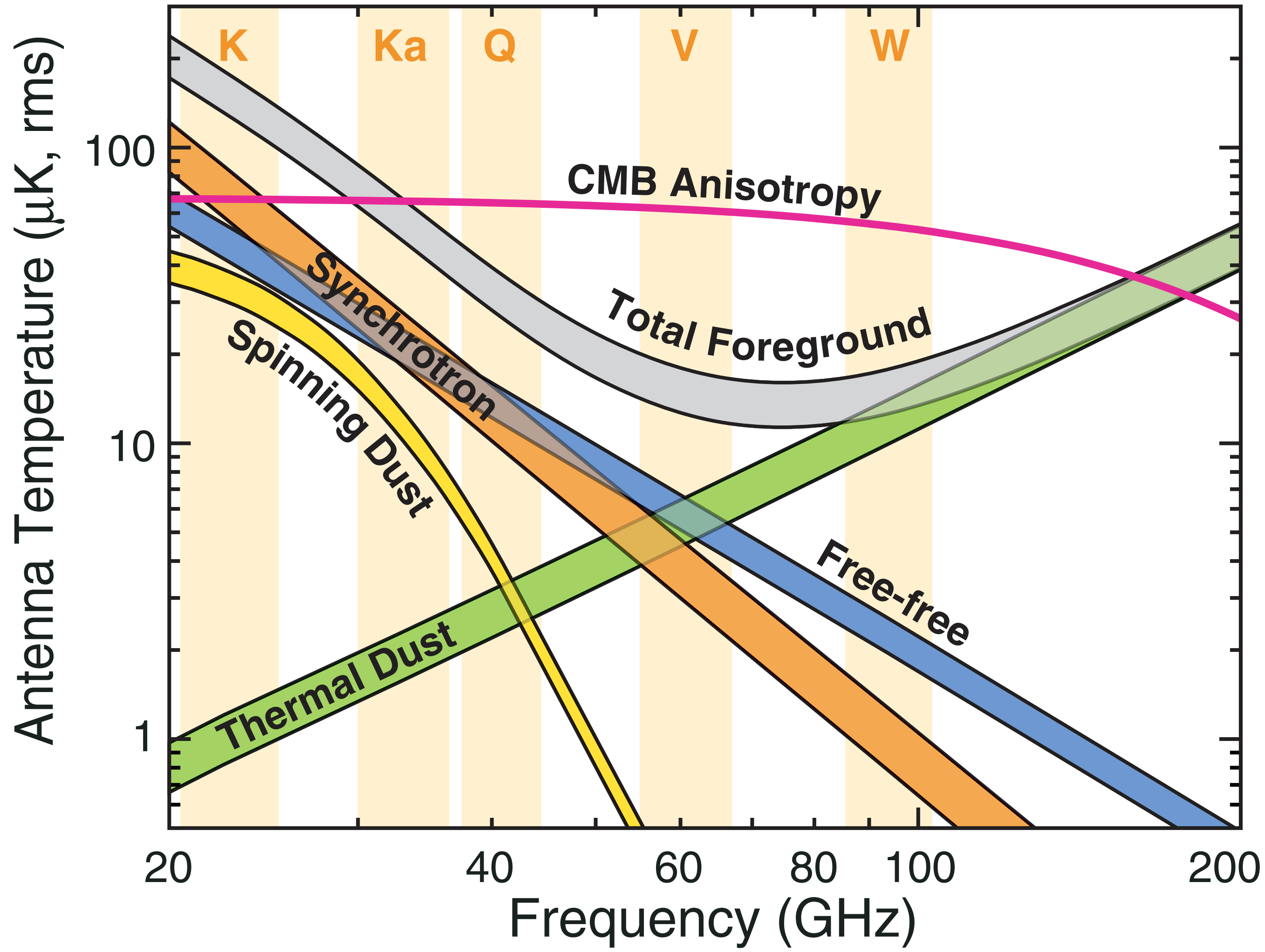

Fig. 22.— Spectra of CMB and foreground anisotropy. The foreground anisotropy results are averages over the three foreground models (MCMCg, MEM, and Model 9). The upper curve for each foreground component shows results for pixels outside of the KQ85 mask, and the lower curve shows results outside of the KQ75 mask. The different foreground models are in good agreement for the total foreground anisotropy. Results for the individual foreground components depend on model assumptions discussed in the text, and typically differ among the three models by 5% to 25%.

(A color version of this figure is available in the online journal.)

Nine-Year Wilkinson Microwave Anisotropy Probe (*WMAP*) Observations: Final Maps and Results

C. L. Bennett[1], D. Larson[1], J. L. Weiland[1], N. Jarosik[2], G. Hinshaw[3], N. Odegard[4], K. M. Smith[5,6], R. S. Hill[4], B. Gold[7], M. Halpern[3], E. Komatsu[8,9,10], M. R. Nolta[11], L. Page[2], D. N. Spergel[6,9], E. Wollack[12], J. Dunkley[13], A. Kogut[12], M. Limon[14], S. S. Meyer[15], G. S. Tucker[16], E. L. Wright[17]